Spectral and electron-collision properties of atomic ions: Threshold phase shifts

Constantine E. Theodosiou
Department of Physics and Astronomy, The University of Toledo, Toledo, Ohio 43606

Steven T. Manson
Department of Physics and Astronomy, Georgia State University, Atlanta, Georgia 30303

Mitio Inokuti
Argonne National Laboratory, Argonne, Illinois 60439
(Received 6 November 1985)

Threshold phase shifts (or equivalently, quantum defects at the series limit) are calculated within the framework of the Hartree-Slater (central-field) approximation for positive atomic ions with nuclear charge number $Z \leq 37$. The results are displayed in isoelectronic (the number of electrons, N, constant), isonuclear (Z constant), and isoionic ($Z-N$ constant) pictures. The systematics of the threshold phase shifts are delineated, and the utility of each of the pictures is discussed. The possibilities and pitfalls of interpolation to generate new data are also discussed. This paper represents the initial report of a systematic investigation of ionic properties.

I. INTRODUCTION

The advent of heavy-ion accelerators and of beam-foil spectroscopy has given a great impetus to the theory of both electron collisions and spectroscopy of atomic ions. Furthermore, the physics of some highly stripped ions finds application in controlled thermonuclear research and astrophysics. The recent heightened interest in this general subject has stimulated us to extend our ongoing study into the systematics of the properties of neutral atoms to the relatively unexplored area of atomic ions.

We stress the point of view, based on extensive experience with neutrals, particularly in the context of quantum-defect theory,[1-3] that diverse observable data can be usefully represented in terms of a limited set of key numerical parameters (e.g., phase shifts, oscillator strength densities, and amplitudes at the nucleus). The variation of such parameters from one ion species to another lends itself to easy and instructive mapping using realistic atomic models. By so mapping these parameters throughout the entire periodic system and for all ionic charges, we hope to establish trends that will form a reliable basis for predicting unmeasured properties of ions. Moreover, this survey is useful for establishing to what extent such well-known spectral features as Cooper zeros and shape resonances,[4] so important in neutral atoms, control the spectral behavior of ions.

Any property of ions can be considered as a function of two variables, the nuclear-charge number (or atomic number) Z and the number of electrons N. Therefore, our data can be analyzed in terms of at least three alternative pictures: *isoelectronic* (N kept constant), *isonuclear* (Z kept constant), and *isoionic* ($z=Z-N+1$ kept constant). Note that the spectroscopist calls z the order of the spectrum and that an electron at large distances sees a Coulomb potential due to the net charge ze. Each of these pictures brings out different aspects of the variation of a given quantity over Z and N.

The *isoelectronic* picture is the most straightforward from a computational view point and is widely used. In addition, it is closely related to the $1/Z$ expansions.[5] Each of the properties approaches the known hydrogenic values asymptotically[6] when plotted against $1/Z$ ($1/Z \rightarrow 0$). The *isonuclear* picture simplifies the variation of ionic properties from one order of the spectrum to the next. Further, the *isonuclear* picture is the most suitable for certain applications. For example, if we consider a given impurity contamination in a fusion plasma, the many ions of that impurity nuclide which are relevant constitute an isonuclear sequence. This is also true for astrophysical applications.[7] The *isoionic* picture maintains a constant asymptotic potential $-ze^2/r$ seen by an electron, and focuses on the interplay between increasing Z and increasing N. This provides a framework for the transfer of the extensive experience with neutral atoms, $z=1$, gained by traditional spectroscopy and collision physics.

At an ionization threshold there is a union between discrete states, usually characterized by their quantum defects and treated by spectroscopic methods, and continuum states, usually characterized by their scattering phase shifts and treated by collision theory. Quantum-defect theory[1-3] shows, among other things, that these two manifolds of states are smoothly connected when the data are suitably renormalized. This reveals the Rydberg series to be an appendage to the continuum so that the most basic wave-function parameters, viz., phase and amplitude, vary smoothly through threshold. In particular, the quantum defect μ_l at the limit of the Rydberg series and the zero-energy scattering phase shift δ_l (with respect to the Coulomb phase) are related simply by

$$\pi\mu_l(n \rightarrow \infty) = \delta_l(E=0), \tag{1}$$

where l is the orbital angular-momentum quantum num-

ber, and n is the principal quantum number. In approaching the problem of mapping out the behavior of phase shifts as a function of both atomic number and ionic charge, we decided to begin by limiting the scope of the study to a single standard energy. We have chosen as our standard energy the ionization limit where the asymptotic kinetic energy E of the one-electron states equals zero. Consequently, our discussion pertains directly to properties of nearby states both below and above the threshold for ionization.

Calculations have been performed, employing single-channel central-field wave functions, for s, p, d, and f waves with $Z \leq 37$ and all states of ionization, i.e., $1 \leq z \leq Z$. In Sec. II a brief review of the theory is given. Section III presents and discusses our results in each of the pictures described above. The final section gives a summary and conclusions.

II. BRIEF REVIEW OF THEORY

The threshold phase shifts were obtained by calculating the continuum wave function at zero energy and using standard methods to extract $\delta_l(0)$ $(=\pi\mu_l)$.[1-3,8] Specifically, the method described in Sec. VIII of Ref. 9 was used to obtain phase shifts accurately. Hartree-Slater (HS) wave functions were used in this study.[10,11] The HS central-field model was used since it is quite amenable to large-scale calculation. In addition, HS functions have been shown to be reasonably accurate for the neutrals;[8,9] the accuracy can be expected to be even better for positive ions.

To understand this point, consider the potential for electrons in an ion of atomic number Z and N electrons, i.e.,

$$V=-\sum_{i=1}^{N}\frac{Ze^2}{r_i}+\sum_{\substack{i,j\\(i<j)}}^{N}\frac{e^2}{r_{ij}}=Z\left[-\sum_{i=1}^{N}\frac{e^2}{r_i}+\frac{1}{Z}\sum_{\substack{i,j\\(i<j)}}^{N}\frac{e^2}{r_{ij}}\right]. \tag{2}$$

For a fixed N, it is clear that the $1/Z$ coefficient of the second term in large parentheses in Eq. (2) causes it to decrease in magnitude relative to the first term, with increasing Z. Since this second term, the noncentral interelectron repulsion, is precisely the part of the potential which is being approximated in the central-field model, it is apparent that the approximation gets better as Z increases and the nuclear attraction dominates. We thus expect our results for highly charged positive ions to be quite accurate.

Note that within the framework of our calculations neither multiplet splitting nor spin-orbit effects are included. Therefore, our results should be viewed as representing an average over the multiplet and fine-structure components of a configuration.

It is true that the single-channel central-field approximation is not the most advanced method for treating atomic dynamics, but the results one obtains from it are often extremely useful and indeed help one understand major features of atomic spectra. Indeed, the work of Manson[8] on neutral atoms has proved valuable as a starting point of the interpretation of many experimental data. The present paper is an extension of that work to stripped ions, for which the single-channel approximation should be even more realistic for reasons discussed above. For an open-shell system, sometimes spectra are influenced by configuration effects and channel-coupling effects, which are beyond the scope of our calculations. Yet, to begin a serious analysis of those effects, one must have full information about results from a single-channel treatment. In this sense, the present paper provides a groundwork for more advanced studies.

III. RESULTS AND DISCUSSION

Threshold phase shifts (or equivalently, quantum defects at the series limit) have been calculated for s, p, d, and f waves for *all* the positive ions of *all* of the atoms with atomic number $Z \leq 37$. For purposes of comparison, the neutrals have been included as well. For each atom and ion, we treat the motion of an electron in the field of the *ground-state* core.

A. Isoionic picture

A selection of the quantum-defect results are shown in the isoionic picture ($z=Z-N+1=$const) in Fig. 1. The

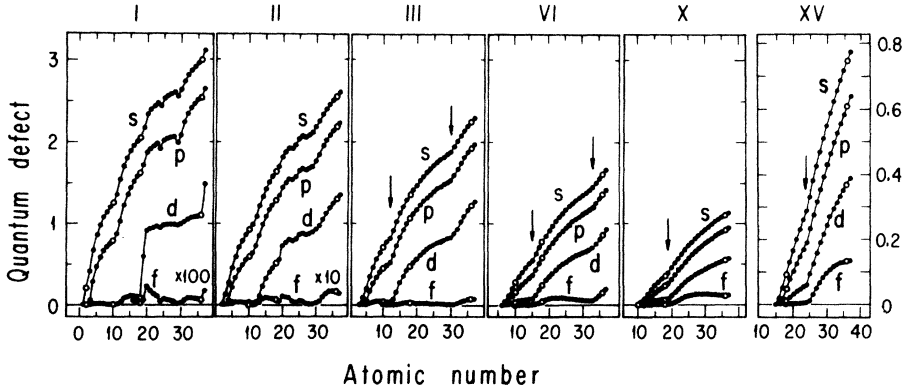

FIG. 1. *Isoionic* pictures of the zero-energy phase shift in units of π (quantum defect μ_l at the series limit). The Roman numerals indicate the order of the spectrum, or $z=Z-N+1$. The arrows indicate the positions of the hydrogenic magic numbers, while the open circles denote noble-gas nuclides. Note the change of vertical scale on the rightmost panel.

variation of each of the μ_l's with Z for the neutrals ($z=1$), or the first spectrum, is seen to be rich in structure. This structure is associated with the chemical properties of the elements. For the second spectrum ($z=2$), this structure persists, but to a much lesser extent. For $z \geq 3$, on the other hand, Fig. 1 shows that this rich structure has completely disappeared.

The structure for $z=1$ is due to the delicate balance among the forces acting on an electron: the electrostatic forces of nuclear attraction and interelectron repulsion, and the centrifugal repulsion. This causes, among other things, the special filling of subshells at $Z=24$ ($4s\,3d^5$) and at $Z=29$ ($4s\,3d^{10}$) leading to a tighter core (because $3d$ orbitals are smaller than $4s$) and, consequently, to greater screening of an excited electron. This increased screening makes the net force on the electron less attractive, thus decreasing μ_l as seen in Fig. 1. In addition, μ_d is seen to be more or less a step function for $z=1$ with steps beginning at $Z=18$ and 36, i.e., for the noble gases. These steps are a consequence of the effective d-wave potential which has an inner well and an outer well separated by a barrier.[12] For $Z \leq 18$, the d waves cannot penetrate the barrier and therefore do not sample the nonhydrogenic inner part of the potential. In the outer region in which the wave function has appreciable amplitude, the potential is virtually hydrogenic. Thus μ_d is quite small for $Z \leq 18$. By $Z=20$, the first loop of the d wave moves into the inner region and μ_d rises to almost unity and again remains roughly constant up to $Z=36$, above which the steplike structure repeats itself. The behavior of the μ_l's for $z=1$ over the entire Periodic Table is discussed in more detail elsewhere.[8,9]

For the $z=2$ results, the dips in μ_l associated with the special filling pattern, e.g., at $Z=24$ and 29, are much smaller, and the step structure of μ_d has all but disappeared. Both are due to the decrease in interelectron repulsion, owing to the loss of one electron, which makes the potential more attractive. Only a vestige of the effect that led to the anomalous filling remains, and the effective d-wave potential no longer has a double well in general. For $z \geq 3$, the nuclear attraction dominates the potential and no jump or nonmonotonic behavior is seen as a result. Further, it is seen that the μ_l's are becoming smaller, with increasing z, which further indicates the increasing dominance of the nuclear attraction and the resulting approach to the hydrogenic behavior. For $z=Z$, the one-electron systems, all the μ_l's, of course, are zero.

It is also evident from Fig. 1 that for $z=1$, the slopes of the μ_l versus Z curves display discontinuities. These occur when the number of electrons N is 2, 10, 18, and 36, i.e., for the closed-shell systems. For $z=2$ one observes some changes in the slope discontinuities and by $z=3$ a new pattern emerges: changes in slope are now seen at $N=2$, 10, and 28, but not at $N=18$ or 36. In other words, as the stage of ionization increases, the magic numbers occur no longer at the noble gases, but rather at the hydrogenic closed-shell systems. For example, $N=18$ is a magic number for the neutrals, having a filled $3p$ subshell. In contrast, for multicharged ions with the dominance of the nuclear attraction, the closed-shell system does not occur until the $3d$ is also filled, i.e., until $N=28$. This is precisely what is seen in Fig. 1. Accordingly, we would expect that similar behavior will be observed for ions at $N=60$ where the $n=4$ shell is filled. Sample calculations (not shown) confirm this point.

Existing experimental data on atomic ions are distressingly fragmentary. Thus, it is of importance to scrutinize the possibility of interpolation in the isoionic picture. Generally, interpolation can be accomplished well only if the curve is smooth. For $z=1$ and 2, the μ_l's are certainly not very smooth as a function of Z, and thus are not amenable to interpolation. Fortunately, however, these are just the cases where experimental data are most abundant. For $z=3$ and higher stages of ionization, the μ_l versus Z curves are smooth except for the changes in slope at the electron numbers corresponding to the hydrogenic filled shells. Thus, interpolation can be done reasonably well *between* $N=2$, 10, 28, and 60, but not across these values of N. From the point of view of interpolation and systematics of ionic data, then, a high-priority item should be acquisition of experimental data for 2-, 10-, 28-, and 60-electron systems.

B. Isonuclear picture

Another way to look at these results is in the *isonuclear* picture, where Z is held constant and the μ_l's are plotted against z. Selected results in this picture are shown in Fig. 2. For all Z, μ_s and μ_p decrease monotonically as z increases; μ_d and μ_f are decreasing for large enough z, but not necessarily for small z. Of course, $\mu_l=0$ for $z=Z$ (the one-electron ions), and thus we know that μ_l *must* be decreasing for large enough z. At low z, the rising or falling behavior of μ_d depends on the potential in each case, which determines whether or not the d wave penetrates the ion core at threshold. The μ_f always rise for small z in all cases considered. This is because the f wave is kept from the ion core at $z=1$ by the centrifugal barrier. With increasing z, the nuclear attraction becomes more dominant and the f wave penetrates the non-Coulomb region of the potential, giving rise to an increasing μ_f. Thus, the results presented in the *isonuclear* picture are explained in the same way as in the *isoionic* picture.

Note that the isonuclear results also show the discontinuities in slope at the hydrogenic magic numbers. This is most pronounced for the higher l's. In fact, μ_f for $Z=37$ shows a change in sign of the slope at $N=28$ ($z=10$). Aside from these points, the curves are quite smooth for $z \geq 3$, indicating that interpolation should be quite easy between the magic numbers.

C. Isoelectronic picture

This is usually a representation of atomic properties that shows the smoothest behavior as a function of the atomic number: the number of electrons remains constant and the increased nuclear charge simply pulls all the electrons closer to the origin. This general property has made the isoelectronic behavior a favorite subject of theoretical studies because in many computational schemes the formalism may be kept exactly the same for members of a

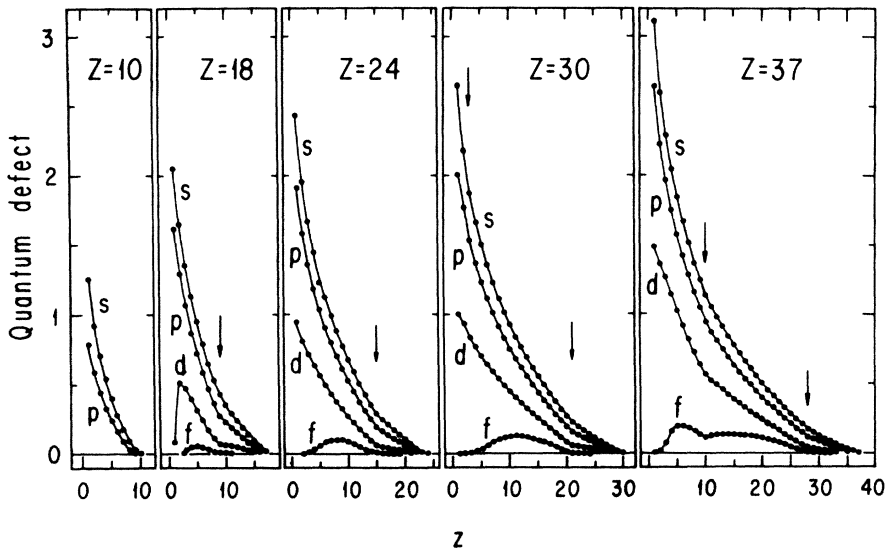

FIG. 2. *Isonuclear* pictures of asymptotic quantum defects vs $z = Z - N + 1$. The arrows indicate hydrogenic magic numbers.

sequence. A sample of our results, depicted in this fashion in Fig. 3(a), verifies the expected smooth behavior of phase shifts. Within the range of atomic numbers studied, μ_s and μ_p always decrease with increasing Z. The μ_d sometimes rise before the asymptotic decrease and the μ_f rise in *all* the cases we studied, before they eventually decrease. As discussed above, the behavior of μ_d and μ_f is strongly affected by the interplay of the centrifugal forces with the attractive electrostatic forces, which in turn depends on how close an ion is to the complete filling of a (sub)shell. Because the number of electrons N remains the same along the sequence, we neither expect nor find any changes in the slope of the curves due to hydrogenic magic numbers.

As Z increases while N is kept constant, the ratio of the nuclear term to the electron-electron repulsion term in Eq. (2) increases. This leads to the general shrinking of all core-electron clouds, and thence to the eventual decrease in all quantum defects at large Z. In other words, increasing Z results in a more effective shielding of the nucleus, and thence in reduced core penetration by the active electron, i.e., reduced quantum defect (or phase shift).

One of the major advantages of the isoelectronic picture is that one can dependably carry out interpolations from existing values of atomic parameters. From the discussion above, it is obvious that all μ_l's go to zero as Z goes to infinity [c.f. Eq. (2)]. This fact can be utilized to provide a significant extra data point. From Fig. 3(b), where we plot $Z\mu_l$ versus $1/Z$ for the sample case of $N = 15$, it is clear that we can dependably interpolate and find the values of all μ_l, $l = 0$–3, for all $Z \lesssim 37$.

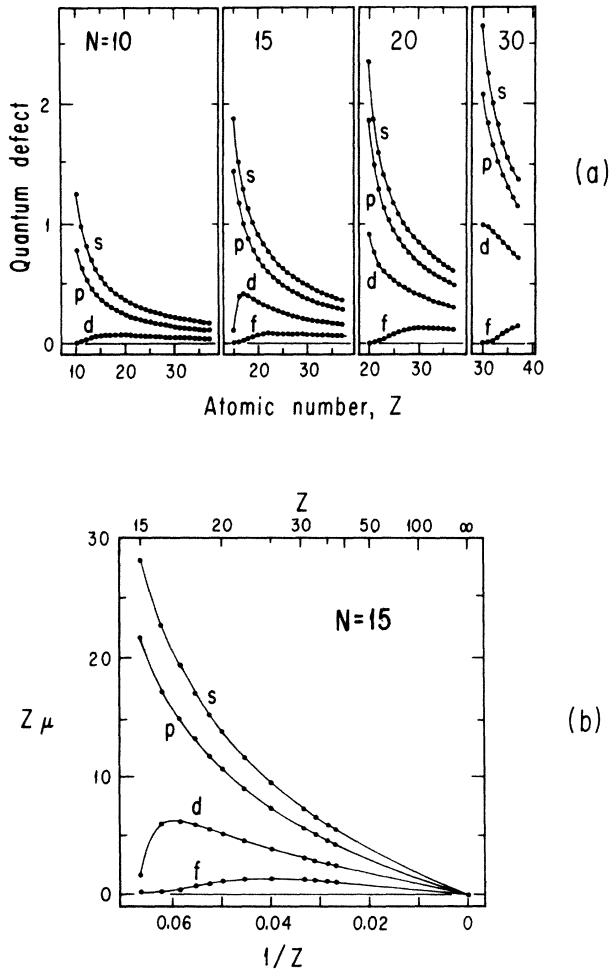

FIG. 3. (a) *Isoelectronic* pictures of quantum defects μ_l. (b) The same picture for $N = 15$ redrawn to include the $Z = \infty$ point. Interpolation for $Z < \infty$ is obviously dependable.

D. Overall picture

To focus on the global behavior of the quantum defects, we present three-dimensional graphs of the functions

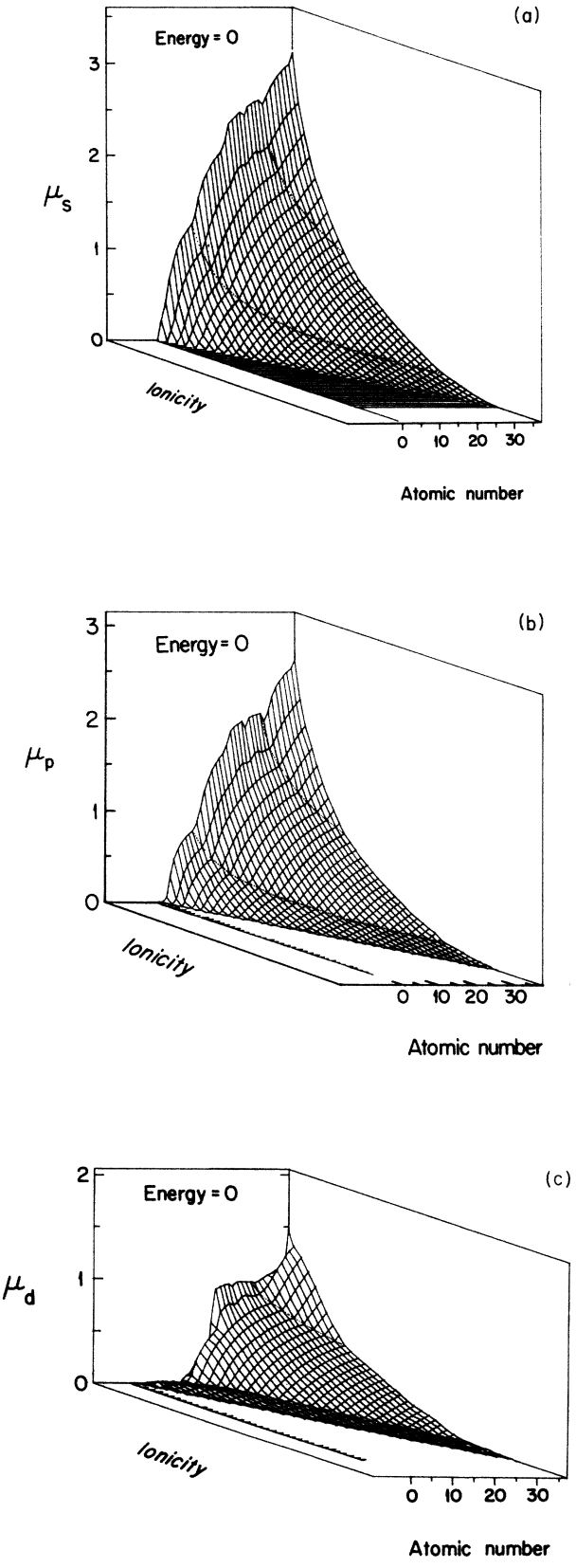

FIG. 4. Quantum defects vs atomic number Z and ionicity: (a) s waves, (b) p waves, (c) d waves. The dotted lines trace the locations of ions with a hydrogenic magic number of electrons.

$\mu_l(Z,z)$ in Fig. 4. The pictures discussed in Secs. III A–III C represent various ways of intersecting these three-dimensional surfaces with a plane. These surfaces reflect the qualitative behavior of the μ_l rather than the details.

Comparing the three surfaces in Figs. 4(a)–4(c), it is clear that, for a given (Z,z), μ_l decreases with increasing l, i.e., $\mu_l > \mu_{l+1}$. This is a consequence of the repulsive centrifugal potential $\hbar^2 l(l+1)/2mr^2$, which makes the effective potential less attractive with increasing angular momentum.

The outstanding substructures on the surfaces in Fig. 4 are the creases along the isoelectronic paths $N = Z - z + 1 = 10$ or 28, the hydrogenic magic numbers. As discussed above, these electron numbers correspond to the closing of the L and M shell, respectively, within the *hydrogenic* ordering of subshells, and do not correspond to the most stable neutral electron numbers of 10 and 18. This closed-shell stability will be reflected in many other atomic parameters that will be discussed elsewhere. Ions in these isoelectronic sequences represent the starting points for upturns in the function $\mu_l(Z,z)$ with increasing Z. This is most clearly observed in the $l = 1,2$ surfaces and is due to the starting of a new shell in the core which adds to the phase-shift- (quantum-defect-) producing capacity of the potential.[9] Because of the generally larger penetration of lower-l wave functions, reflected in their larger quantum defects, the magic-number crease is less pronounced for low l than for high l. The crease is most dramatic at the $N = 10$ isoelectronic cut for $l = 2$, where μ_d remains vanishingly small until the $n = 3$ shell begins to fill. Owing to the large centrifugal repulsion for $l = 2$, d waves have significant penetration only as close to the nucleus as the M shell. Consequently, the core must contain an M electron before the $l = 2$ phase shift departs appreciably from the hydrogenic limit. In contrast, substantial departure of μ_f from zero is delayed until $Z - z > 60$, which accounts for the absence of an $l = 3$ surface.

E. Comparison with experiment

For several isoelectronic sequences, we have compared calculated quantum defects μ_l with values derived from spectroscopic data.[13–28] Tables I–V illustrate some examples. It is elementary to convert a spectroscopic term value to the quantum-defect value $\mu_l(n)$ at each principal quantum number n. When the data are available for a series of terms with varying n for a fixed l, it is usually easy to determine the limit μ_l as $n \to \infty$, to a precision better than shown in Tables I–V. Generally the data for several n values suffice for the purpose.

As Table I shows, the calculated μ_l for the sodium sequence agree within 0.02 for all l. The agreement is a little poorer for $l = 2$, but the calculated values still serve as an excellent guide to the trend of spectroscopic data. For $l = 3$ the difference between calculated and experimental values is exceedingly small (≤ 0.004). In terms of percentages, on the other hand, there are sometimes substantial differences particularly for the lower Z's where μ_f is exceedingly small.

TABLE I. Quantum defects for the sodium-isoelectronic sequence ($N=11$). To derive experimental values of μ_l, we have used spectroscopic data given by Refs. 13–27 and by Lindgård and Nielsen, Ref. 28.

Spectrum	Z	z	l	μ_l HS calculation	Experiment	Remarks
Na I	11	1	0	1.359	1.35	
			1	0.867	0.85	
			2	0.0069	0.012	
			3	0.000 05	0.001	
Mg II	12	2	0	1.082	1.07	
			1	0.717	0.70	
			2	0.038	0.045	
			3	0.0005	0.003	
Al III	13	3	0	0.910	0.90	
			1	0.613	0.60	
			2	0.075	0.073	
			3	0.002	0.006	
Si IV	14	4	0	0.790	0.78	
			1	0.537	0.51	
			2	0.100	0.089	
			3	0.003	0.006	
P V	15	5	0	0.700	0.69	
			1	0.478	0.45	
			2	0.114	0.097	
			3	0.005	0.008	
S VI	16	6	0	0.629	0.61	
			1	0.431	0.41	
			2	0.119	0.099	
			3	0.007	0.008	
Cl VII	17	7	0	0.572	0.57	
			1	0.393	0.318	
			2	0.120	0.092	
			3	0.008	0.008	
Ar VIII	18	8	0	0.525	0.52	
			1	0.361	0.35	
			2	0.118	0.10	
			3	0.010	0.006	
K IX	19	9	0	0.485	0.48	
			1	0.334	0.32	
			2	0.115	0.096	
			3	0.011	0.011	
Ca X	20	10	0	0.450	0.44	
			1	0.311	0.30	
			2	0.112	0.093	
			3	0.012	0.012	
Sc XI	21	11	0	0.421	0.42	
			1	0.291	0.28	
			2	0.108	0.094	
			3	0.012	0.010	
Ti XII	22	12	0	0.395	0.39	
			1	0.273	0.26	
			2	0.104	0.085	
			3	0.013	0.010	

TABLE I. (*Continued*).

Spectrum	Z	z	l	μ_l HS calculation	Experiment	Remarks
V XIII	23	13	0	0.373	0.38	
			1	0.258	0.25	
			2	0.100	0.080	
			3	0.013	0.05	Scanty experimental data
Cr XIV	24	14	0	0.352	0.36	
			1	0.244	0.24	
			2	0.097	0.077	
			3	0.013	0.008	
Mn XV	25	15	0	0.334	0.34	
			1	0.231	0.23	
			2	0.093	0.08	
			3	0.013	0.007	Scanty experimental data
Fe XVI	26	16	0	0.318	0.32	
			1	0.220	0.21	
			2	0.090	0.076	
			3	0.014	0.012	

TABLE II. Quantum defects for the magnesium isoelectronic sequence ($N=12$).

Spectrum	Z	z	l	μ_l HS calculation	Experiment	Remarks
Mg I	12	1	0	1.54	1.60	
			1	1.03	1.13	
			2	0.029	0.28	
			3	0.0003	0.05	
Al II	13	2	0	1.215	1.26	
			1	0.851	0.90	
			2	0.109	0.20	
			3	0.003	0.02	Series perturbation
Si III	14	3	0	1.022	1.05	
			1	0.726	0.77	
			2	0.162	0.22	
P IV	15	4	0	0.888	0.89	
			1	0.635	0.67	
			2	0.182	0.16	
S V	16	5	0	0.788	0.83	
			1	0.565	0.64	
			2	0.186	0.20	
Cl VI	17	6	0	0.710	0.74	
			1	0.510	0.59	
			2	0.183	0.17	
K VIII	19	8	0	0.594	0.595	
			1	0.428	0.42	
			2	0.170	0.17	
			3	0.027	0.029	

TABLE III. Quantum defects for the aluminum isoelectronic sequence ($N=13$).

Spectrum	Z	z	l	μ_l HS calculation	Experiment	Remarks
Al I	13	1	0	1.697	1.77	
			1	1.230	1.34	
			2	0.0736	0.059	
			3	0.0008	0.036	
Si II	14	2	0	1.336	1.40	
			1	0.986	1.04	
			2	0.225	0.24	
P III	15	3	0	1.125	1.17	
			1	0.834	0.89	
			2	0.266	0.20	
S IV	16	4	0	0.980	0.97	
			1	0.727	0.80	Scanty data
			2	0.266	0.25	
Cl V	17	5	0	0.871	0.93	
			1	0.647	0.76	Scanty data
			2	0.256	0.27	
Ar VI	18	6	0	0.786	0.84	Scanty data
			1	0.584	0.6	
			2	0.243	0.3	

The agreement of the calculated values with experiment improves with increasing $z=Z-N+1$ so long as z is not very large. This is so because, with increasing z, the dynamics of electron motion is more and more dominated by the central force, and thus becomes simpler; then, the HS potential model should be better applicable for larger z (until relativity effects become appreciable). Yet, at very high stages of ionization (e.g., for z greater than 13 in the sodium-isoelectronic sequence), the agreement deteriorates, most likely because spectroscopic data tend to be progressively scarce and thus uncertain. In other words, the HS results are probably more reliable than current experimental data for those high-z values.

Table II shows selected data for the magnesium

TABLE IV. Quantum defects for the potassium isoelectronic sequence ($N=19$).

Spectrum	Z	z	l	μ_l HS calculation	Experiment	Remarks
K I	19	1	0	2.177	2.18	
			1	1.712	1.71	
			2	0.595	0.27	
			3	0.0006	0.011	
Ca II	20	2	0	1.811	1.81	
			1	1.451	1.45	
			2	0.719	0.63	
			3	0.010	0.027	
Sc III	21	3	0	1.532	1.57	Scanty data
			1	1.229	1.27	
			2	0.611	0.61	
			3	0.019	0.05	
Fe VIII	26	8	0	0.969		Data unavailable
			1	0.779	0.8	Scanty data
			2	0.437	0.4	
			3	0.111	0.12	

TABLE V. Quantum defects for the calcium isonuclear sequence ($Z=20$).

Spectrum	N	z	l	μ_l HS calculation	μ_l Experiment	Remarks
Ca I	20	1	0	2.346	2.42	
			1	1.871	1.93	
			2	0.909	0.95	
			3	0.002	0.09	
Ca II	19	2	0	1.811	1.81	
			1	1.451	1.45	
			2	0.719	0.63	
			3	0.010	0.027	
Ca III	18	3	0	1.472	1.39	Beginning of the
			1	1.173	1.24	open-shell core,
			2	0.560	0.30	and thence multiplet
			3	0.019	0.0045	structure
Ca IV	17	4	0	1.256	1.30	Average over multiplets
			1	0.994	0.95	
			2	0.487		Data unavailable
			3	0.044		
Ca VIII	13	8	0	0.659	0.69	
			1	0.490		Data unavailable
			2	0.218	0.19	
			3	0.051	0.02	
Ca IX	12	9	0	0.550	0.56	
			1	0.396	0.40	
			2	0.163	0.16	
			3	0.029	0.034	
Ca X	11	10	0	0.451	0.44	
			1	0.311	0.30	
			2	0.112	0.093	
			3	0.012	0.012	

isoelectronic sequence. One sees here the same general trends as with the sodium isoelectronic sequence. The calculated quantum defects for $l=0$ and $l=1$ are fairly close to experiment even at $z=1$ and 2, and are excellent for $z\geq 3$. The calculated values for $l=2$ also agree well with experiment at $z\geq 3$. Finally, we observe that the degree of overall agreement between the calculation and experiment is about the same for the magnesium isoelectronic sequence as for the sodium isoelectronic sequence. This is somewhat surprising because one would expect better agreement for the sodium isoelectronic sequence, for which the notion of the single-channel quantum defect is better applicable.

When there are two or more electrons outside the ion core, the comparison is not quite straightforward because of the multiplet structure of energy levels; a full analysis of spectroscopic data would require a multichannel treatment. We have compared the calculated μ_l values with an estimate of the mean value of the quantum defect over the multiplet members. More specifically, when the term values for all the multiplet members are known, we first deduced the quantum-defect values for each member, and then calculated the mean of them with the statistical weights of the members. After we carried this out for several values of n in a given series of l, we determined the quantum defect at the series limit. Sometimes not all the multiplet members have been identified, especially for higher principal quantum numbers n, which are most pertinent to the quantum-defect determination. In this case, the mean value of the quantum defect for the multiplet had to be guessed from fragmentary data, as we indicate in the remarks of Tables I–V. We also note in the remarks those cases where there are signs of series perturbations and other reasons for uncertainties in the derived quantum-defect values.

Table III shows comparison of the calculation with experiment for the beginning members of the aluminum isoelectronic sequence. Again, the agreement of the calculated values with experiment is fair for $z=1$ and 2, and becomes closer for higher z. In this connection, we note the following two points. First, the idea of the single-channel quantum defect is a too-simplistic approximation for the three-electron configuration $3s^2nl$ in general, and especially for lower z. Second, the quantity and perhaps

the quality of experimental data tend to deteriorate for higher z; indeed, the HS values are probably powerful in predicting μ_l for $z \geq 4$ and for n greater than about 5.

Table IV shows a very limited selection of data on the potassium isoelectronic sequence. The agreement between the calculation and experiment is fair or good for $z \geq 2$, whenever we can find experimental data. This isoelectronic sequence is characterized by the configuration $3p^6nl$, and thus should be well described in terms of the single-channel quantum-defect theory. Therefore, our calculation should be reliable for predicting term values for higher z. For instance, our quantum defect values for Fe VIII should serve as a powerful guide for locating unobserved energy levels.

There is a notable discrepancy for the μ_d values for K I. Indeed, this discrepancy is the largest we have ever found during the comparison between theory and experiment. Indeed, we have been aware of the peculiarity of this particular case, from studies[29–31] on other properties. The discrepancy arises because the effective potential for the d wave in the field of the neutral potassium has two shallow wells separated by a maximum. As a result, the zero-energy wave function, as evaluated in the HS model, represents an intermediate between an inner-well state and an outer-well state. Therefore, a slight modification of the effective potential would result in a large change in the phase shift, or the quantum defect. In conclusion, the HS potential used in our calculation is somewhat too attractive, and thus leads to the excessively large value of the quantum defect.

Finally, Table V shows the comparison of our calculation with experiment[19] for the calcium-*isonuclear* sequence. For $z=1$ and 2, we see the same trend as noted before. Indeed, the entries for $N=19$ ($z=2$, Ca II) are the same as in Table IV. When we look at data in the isonuclear sequence, we find that the agreement of our calculation with experiment does not steadily improve with increasing z. At $z=3$ (Ca III), the agreement is much poorer than at $z=1$ or 2. This is well understandable once we recall the electronic shell structure. At $z=3$, the relevant electron configuration is $3p^5nl$; in other words, at $z=3$ one begins to see the open-shell ion core, which leads to multiplet structure of energy levels. As a consequence, the notion of the single-channel quantum defect becomes less applicable here than for $z=1$ ($3p^6nl^2$) or for $z=2$ ($3p^6nl$).

At $z=8$, the agreement of our calculation with experiment becomes good again. Here the electron configuration is $2p^63s^2nl$, and therefore the single-channel quantum-defect theory again applies. For $z=9$, the electron configuration is $3p^63snl$; for $z=10$ it is $3p^6nl$. Therefore, our calculation should be more and more realistic. Indeed, the data shown in Table V are consistent with this expectation, and attest to the correctness of our interpretation.

IV. FINAL REMARKS

The systematics of threshold phase shifts for s, p, d, and f waves for positive atomic ions with $Z \leq 37$ have been elucidated. The *isoionic* and *isonuclear* pictures bring out aspects of the systematics that are not apparent in the traditional *isoelectronic* picture; most notably, the rich structure of the periodic system, associated with the chemical properties of the neutral atoms, rapidly disappears in going to multicharged ions, and the magic numbers associated with increased stability change from the noble-gas electron numbers 2,10,18,36,54 for the neutrals, to the hydrogenic 2,10,28,60 associated with the filling of shells of principal quantum numbers $n=1,2,3,4$. The utility of these other pictures is thus evident.

In the comparison of our results with experiment, we have noted irregularities in experimental quantum defects for high members of certain Rydberg series. These irregularities, which show up most clearly when the data are presented as quantum defects, are likely due to external perturbations such as collisions and electromagnetic fields. In these cases, we feel that the theoretical quantum defects may be used to obtain more accurate term values. With this purpose in mind, a comprehensive tabulation of the quantum defects discussed in this paper is presented separately.[32]

ACKNOWLEDGMENTS

We are grateful to Ugo Fano and J. L. Dehmer for their important contributions to the early stages of this work. Several students of Fano also assisted us in the generation and organization of numerical data; among them, Peter D. Persans contributed most. They were supported by the U. S. Department of Energy, Office of Basic Energy Sciences, under Contract No. DE-AS02-76ERO1674. We thank W. C. Martin for valuable discussion about some aspects of spectroscopic data. This work was supported in part by the U. S. Army Research Office and in part by the U. S. Department of Energy, Office of Health and Environmental Research, under Contract No. W-31-109-Eng-38.

[1] M. J. Seaton, Mon. Not. R. Astron. Soc. **118**, 504 (1958).
[2] M. J. Seaton, Rep. Prog. Phys. **46**, 167 (1983).
[3] C. Greene, U. Fano, and G. Strinati, Phys. Rev. A **19**, 1485 (1979).
[4] U. Fano and J. W. Cooper, Rev. Mod. Phys. **40**, 441 (1968).
[5] D. Layzer, Ann. Phys. (N.Y.) **8**, 271 (1959).
[6] M. W. Smith and W. L. Wiese, Astrophys. J. Suppl. **23**, 103 (1973).
[7] B. C. Fawcett, Adv. At. Mol. Phys. **10** 223 (1974).
[8] S. T. Manson, Phys. Rev. **182**, 97 (1969).
[9] U. Fano, C. E. Theodosiou, and J. L. Dehmer, Rev. Mod. Phys. **48**, 49 (1976).
[10] F. Herman and S. Skillman, *Atomic Structure Calculations* (Prentice-Hall, Englewood Cliffs, 1963).
[11] J. P. Desclaux, Comp. Phys. Commun. **1**, 216 (1969).
[12] A. R. P. Rau and U. Fano, Phys, Rev. **167**, 7 (1968).

[13]C. E. Moore, *Atomic Energy Levels,* Natl. Bur. Stand. (U.S.) Circ. No. 467 (U.S. GPO, Washington, D.C., 1949), Vol. I [reissued as Natl. Stand. Ref. Data Ser., Natl. Bur. Stand. (U.S.) Circ. No. 35 (U.S. GPO, Washington, D.C., 1971)].
[14]J. Sugar and C. Corliss, J. Phys. Chem. Ref. Data **6**, 317 (1977).
[15]C. Corliss and J. Sugar, J. Phys. Chem. Ref. Data **6**, 1253 (1977).
[16]J. Sugar and C. Corliss, J. Phys. Chem. Ref. Data **7**, 1191 (1978).
[17]C. Corliss and J. Sugar, J. Phys. Chem. Ref. Data **8**, 1 (1979).
[18]W. C. Martin and R. Zalubas, J. Phys. Chem. Ref. Data **8**, 817 (1979).
[19]J. Sugar and C. Corliss, J. Phys. Chem. Ref. Data **8**, 865 (1979).
[20]C. Corliss and J. Sugar, J. Phys. Chem. Ref. Data **8**, 1109 (1979).
[21]W. C. Martin and R. Zalubas, J. Phys. Chem. Ref. Data **9**, 1 (1980).
[22]J. Sugar and C. Corliss, J. Phys. Chem. Ref. Data **9**, 473 (1980).
[23]W. C. Martin and R. Zalubas, J. Phys. Chem. Ref. Data **10**, 153 (1981).
[24]C. Corliss and J. Sugar, J. Phys. Chem. Ref. Data **10**, 197 (1981).
[25]J. Sugar and C. Corliss, J. Phys. Chem. Ref. Data **10**, 1097 (1981).
[26]C. Corliss and J. Sugar, J. Phys. Chem. Ref. Data **11**, 135 (1982).
[27]W. C. Martin and R. Zalubas, J. Phys. Chem. Ref. Data **12**, 323 (1983).
[28]A. Lindgård and S. E. Nielsen, At. Data Nucl. Data Tables **19**, 533 (1977).
[29]C. E. Theodosiou, J. Phys. B **13**, L1 (1980).
[30]J. Lahiri and S. T. Manson, Bull. Am. Phys. Soc. **28**, 788 (1983); (unpublished).
[31]D. C. Griffin, K. L. Andrew, and R. D. Cowan, Phys. Rev. **177**, 62 (1969).
[32]C. E. Theodosiou, M. Inokuti, and S. T. Manson, At. Data Nucl. Data Tables (to be pubhished).